Applied Catalysis B: Environmental 207 (2017) 267–278

Contents lists available at ScienceDirect

Applied Catalysis B: Environmental

journal homepage: www.elsevier.com/locate/apcatb

Mechanism, kinetics and thermodynamics of carbon dioxide hydrogenation to methanol on $Cu/ZnAl_2O_4$ spinel-type heterogeneous catalysts

Matej Huš*, Venkata D.B.C. Dasireddy, Neja Strah Štefančič, Blaž Likozar

Department of Catalysis and Chemical Reaction Engineering, National Institute of Chemistry, Hajdrihova 19, SI-1000 Ljubljana, Slovenia

ARTICLE INFO

Article history:
Received 26 September 2016
Received in revised form 24 January 2017
Accepted 28 January 2017
Available online 3 February 2017

Keywords:
Hydrogenation
Carbon dioxide
Methanol
Copper–zinc–alumina
Heterogeneous catalyst

ABSTRACT

Heterogeneous catalytic hydrogenation of gaseous carbon dioxide to methanol is an important reduction reaction in chemical process engineering, renewable energy industry and emerging green chemistry, as it provides means to harness surplus electrical energy and convert a pollutant and emitted greenhouse gas into a useful building block and biofuel. On industrial operating scale, multifunctional copper/zinc catalysts on various supporting substrates (*e.g.* CZA with alumina) are most commonly used due to their high selectivity and conversion. In this work, post-Hartree–Fock and density functional theory (DFT) calculations were carried out to assess the thermodynamics and to elucidate the pathway leading to the formation of methanol from CO_2 on realistic spinel-type tri-metallic materials. Firstly, a commercial-like $Cu/ZnO/Al_2O_3$ was synthesised *via* co-precipitation and characterised to obtain the active sites' structure for modelling. Powder X-ray diffraction (XRD), Brunauer–Emmett–Teller (BET) surface area measurement, scanning/transmission electron microscopy (SEM and TEM) and energy-dispersive X-ray spectroscopy (EDS) were performed. Subsequently, the Gibbs free energy, enthalpy, entropy and chemical equilibrium constants of the direct methanol synthesis and the competing reverse water–gas shift (RWGS) reaction at the temperatures of 25, 150, 200, 250 and 300 °C, and the pressures of 1, 20, 40, 60 and 100 bar were evaluated using *ab initio* quantum chemistry method CCSD(T)/aug-cc-pVQZ. To investigate kinetics, a mechanistic pathway scheme with all established intermediates was constructed, whereas physical/chemical adsorption/desorption energies, geometries, barriers and rates for adsorbate elementary steps were calculated using plane-wave DFT. Results demonstrate that the formate precursor route predominates as the respective transition state activation energies are lower and, thus CH_3OH is proposed to form through HCOO, H_2COO, H_2COOH, CH_2O and CH_3O species.

1. Introduction

Despite extensive research effort and considerable advances in technology, using energy-rich carbon–hydrogen bonds remains one of the most efficient means for storing energy. Liquid hydrocarbons are easy to transport and store on one hand and, due to long history of heat engines, convenient to use on the other hand. Additionally, hydrocarbons are useful and valuable raw materials for production of various organic chemicals.

Upon burning hydrocarbons, carbon dioxide is released into the atmosphere. Although not toxic *per se*, its rising atmospheric concentrations have been linked to climate change, raising the Earth surface temperature in a phenomenon called global warming and promoting the acidification of oceans. To mitigate these effects, several approaches have been proposed [1]. As lowering the overall energy consumption is not a feasible proposition, the problem must be tackled two-fold. A transition towards renewable energy sources is underway globally, ushering in the use of hydropower, wind power and solar power. It is not realistic to expect a full transition towards renewable sources soon, therefore ways to remove carbon dioxide from the atmosphere must also be developed. Long-term carbon capture and sequestration is one way to achieve this but finding reliable long-term storage sites has proved difficult.

Green renewable electricity sources also suffer from unpredictable power output, requiring efficient ways to store energy. For instance, on windy and sunny days, production of electrical energy exceeds the demand. Usually, energy output fluctuates, which exerts unwanted stress on the power grid. It would therefore

* Corresponding author.
E-mail address: matej.hus@ki.si (M. Huš).

http://dx.doi.org/10.1016/j.apcatb.2017.01.077
0926-3373/

be beneficial to have a cost-effective way to store this energy in a durable and easy-to-transport form.

Using surplus electrical energy to produce hydrogen from water addresses the challenge of energy storage. However, storage, transportation, and use of hydrogen demand delicate and expensive infrastructure. Utilisation of carbon dioxide to synthesise methanol *via* catalytic carbon dioxide hydrogenation is a possible solution for more efficient energy storage as well as carbon dioxide capture. Methanol that is formed in this way has a neutral carbon footprint and can be used as a very clean source of energy, producing negligible amounts of particulate matter and oxides of nitrogen.

Several industrial methods for methanol production exist. It is mostly produced from syngas mixtures at pressures of up to 100 bar and temperatures between 200 and 300 °C over Cu/ZnO/alumina catalysts. Industrial catalysts are prepared by a co-precipitation method, yielding clusters of active Cu and ZnO nanoparticles on the alumina support [2]. Clusters of Cu are about 10 nm in size and have ZnO nanoparticles interspersed among them [3]. Efficient catalysts have a high Cu:Zn ratio and large surface areas of Cu exposed. It has been already been shown that within the same catalyst family the catalyst activity scales linearly with the accessible Cu surface area [4,5].

Methods for catalyst preparation and the empirical relationships between the catalyst optimisation and activity are disproportionally better understood than the exact mechanism. It is believed that Cu, ZnO and the support act synergistically since the exclusion of any constituent noticeably reduces the catalyst activity [6–8]. Kinks, steps, defects and lattice strain also seem to play a crucial role [2,9].

Several mechanisms for the formation of methanol in the hydrogenation of carbon dioxide have been proposed. As they were put forward based on calculations of varying degrees of simplifications and on very different crystal structures, they differ markedly. A common feature of most of them is their focus on two possible reaction pathways. Depending on the first intermediate formed, the reaction can proceed either *via* the formate route (HCOO, H_2COO, H_2COOH, H_2CO, H_3CO, and CH_3OH) or reverse water–gas shift route (HOCO, CO, HCO, CH_2O, CH_3O, and CH_3OH). There are several other possible intermediates, which are not always included in the discussions.

Behrens et al. showed the HCOO and H_2COO to be the key intermediates over pure Cu(111), Cu(211) and Zn-doped Cu(211) [3]. Zhao et al. argue that on Cu(111) direct hydrogenation does not lead to methanol due to high hydrogenation barriers of HCOO and H_2COO, and instead propose a route through COOH, COHOH, COH, HCOH, and H_2COH, which is catalysed by small amounts of co-adsorbed water on the catalyst [10]. Grabow and Mavrikakis performed extensive density functional theory (DFT) simulations and microkinetic modelling on Cu(111) and found the predominant pathway to include HCOO, HCOOH, H_2COOH, H_2CO and H_3CO intermediates [11]. Studt et al. studied hydrogenation of CO and CO_2 on a stepped copper surface including intermediates HCOO, HCOOH, H_2COO [12]. Calculations on Cu clusters instead on crystals have established HCOO and H_2COO to be the principle intermediates [13]. Yang et al. did DFT calculations and kinetic Monte Carlo modelling on metal-doped Cu (dopants Rh, Ni, Pt, PD, Au) 111 facets. It was found that on pure Cu(111) and Au/Cu(111) the formate pathway predominates, while Pd, Rh, Pt and Ni dopants change the favoured pathway to reverse water–gas-shift [14]. Nakatsuji and Hu studied methanol synthesis on Cu(100) and Zn/Cu(100) and found the formate pathway to predominate [15].

In this work, a comprehensive list of theoretical calculations was carried out to better understand the kinetics and mechanism of the reaction on a complex catalyst. Thermodynamics of carbon dioxide hydrogenation to methanol and the competitive reverse water–gas shift (RWGS) reaction was studied using post-Hartree–Fock quantum chemical methods at different industrially important conditions. For engineering purposes, enthalpy of reaction is usually taken to be constant across a broad temperature range, which is useful, but nevertheless an approximation. Enthalpy, entropy, Gibbs free energy and equilibrium constants were therefore determined and their dependence on temperature and pressure investigated.

To study kinetics of the catalysed reaction, a crystal structure was constructed that to the best of our knowledge mirrored the actual catalyst structure, based on existing literature data and our experimental techniques. A thorough reaction pathway network was put together and investigated using DFT, including less frequently encountered intermediates and reactions on side pathways.

2. Methods

2.1. CCSD(T) calculations

Thermodynamics of carbon dioxide hydrogenation to methanol and RWGS was studied using coupled-clusters singles and doubles theory with perturbative triples corrections (CCSD(T)) [16–21]. Provided a sufficiently large basis set is used, this method is considered a gold standard in accuracy for the theoretical calculations. We used Dunning's correlation-consistent polarised quadruple-zeta basis set with added diffused functions (aug-cc-pVQZ) [22,23], which for first and second period atoms is indistinguishable from the complete-basis-set limit. To obtain true minimum-energy geometries of the reactants and products, an ultrafine pruned grid (99,590) with tight convergence criteria were used in Gaussian 09 program [24].

At pressures 1, 20, 40, 60 and 100 bar and temperatures 25, 150, 200, 250 and 300 °C, partition functions of reactants (H_2, CO_2) and products (CH_3OH, H_2O, CO) were calculated, taking into account zero-point energy corrections, translational, vibrational and rotational motion [25]. These were then used to calculate the enthalpy, entropy and Gibbs free energy of species, ultimately yielding full thermodynamics of the reaction and the equilibrium constants at different conditions from

$$\Delta G^0 = -RT \ln K_p \quad (1)$$

2.2. Plane-wave DFT calculations

Plane-wave based density functional computations were performed using open-source Quantum Espresso program suite [26], which employs PWscf code for calculations of electronic structure. Structures in this paper are visualised with the open-source XCrysDen tool [27].

For description of electronic properties, exchange-correlation functional PBE [28,29] with ultrasoft pseudopotentials obtained from scalar-relativistic calculations and Grimme dispersion correction [30,31] were used. As a sound compromise between the accuracy of the results and the computational cost, a kinetic energy cut-off of 30 Ry for wavefunctions and 300 Ry for charge density and potential was chosen and validated with convergence tests. Due to metallic characters of the catalyst, Gaussian spreading with a width of 0.1 Ry for Brillouin zone integration was selected. Brillouin zone was sampled with 4×4×1 points on a Monkhorst–Pack mesh [32]. Self-consisted cycle was deemed converged when energy change did not exceed 10^{-8} Ry. Geometric optimisation was deemed complete when residual forces dropped below 10^{-3} Ry/au and energy change in an optimisation step was less than 10^{-4} Ry.

Catalyst support was modelled as a slab of four atomic layers of the spinel structure. Slabs in the *z* direction were separated with 15 Å of vacuum. To compensate for spurious interslab interactions,

dipole correction by Bengtsson was employed [33]. Due to a very large unit cell of the spinel structure, a plane with Miller indices 110 of a single unit cell measuring 8.0×11.2 Å sufficed and no supercell was needed (*cf.* Catalyst Structure). Active site was modelled with three copper and three zinc atoms, deposited on top of the spinel support. During the calculations adsorbates, active site, and top two support layers were allowed to relax, while the bottom two layers were kept fixed in their respective bulk positions.

For calculation of molecular species in gaseous phase, a cubic cell with dimension 20×20×20 Å was used. The Brillouin zone was sampled at Γ point and no dipole correction was used.

Transition state structures were determined with nudged elastic band method (NEB) between two stable intermediates [34]. First, an approximate structure was found with NEB and then further refined with climbing image approach until forces orthogonal to the reaction path dropped below 0.05 eV/Å [35]. Transition states were confirmed with vibrational analysis, which revealed exactly one imaginary frequency for each one, corresponding to the movement along the reaction coordinate. Adsorption energies of stable adsorbates, intermediates and transition states were evaluated as

$$\Delta E_{\text{ads}} = E_{\text{species+catalyst}} - E_{\text{catalyst}} - E_{\text{species}} + \Delta E_{\text{ZPE}}. \quad (2)$$

Zero-point energy (ZPE) correction, stemming from the fundamental properties of quantum particles not being able to attain the minimum of classical potential well due to the uncertainty principle, was taken into account as vibrational contribution only

$$\Delta E_{ZPE} = \sum_{i}^{3N} \frac{h\nu_i}{2}. \quad (3)$$

Reaction rates k_{fwd} are calculated from the transition state theory (TST) as

$$k_{fwd} = \frac{k_B T}{h} \frac{q_{vib,TS}}{q_{vib,IS}} \exp\left(-\frac{E_A}{k_B T}\right) \quad (4)$$

where k_B is the Boltzmann constant, T temperature, h Planck constant, E_A activation energy for forward reaction and $q_{vib,TS}$ and $q_{vib,IS}$ vibrational partition functions for transition and initial states, respectively. The latter are calculated as

$$q = \Pi_i^{3N} \frac{1}{1 - e^{-\frac{h\nu_i}{k_B T}}}, \quad (5)$$

while the reaction rates for reverse reactions k_{bwd} follow from the equilibrium constants:

$$K = \frac{k_{fwd}}{k_{bwd}} = \exp\left(\frac{-\Delta E}{k_B T}\right) \quad (6)$$

For adsorption reactions, the forward rate is evaluated from the collision theory, supposing that the sticking probability equals unity, as

$$k_{fwd} = \frac{1}{N_0 \sqrt{2\pi m k_B T}}, \quad (7)$$

where N_0 equals the number of reaction sites per catalyst as $1.9{\cdot}10^{17}\ \text{m}^{-2}$ (derived from hydrogen temperature-programmed desorption) and m is the molecular weight of the species. The reverse rate follows from the equilibrium constant

$$K = \frac{k_{fwd}}{k_{bwd}} = \frac{q_{vib*}}{q_{vib} q_{rot} q_{trans,g}} \exp\left(\frac{-\Delta E_{ads}}{k_B T}\right) \quad (8)$$

where q_{vib}, q_{rot} and q_{trans} denote the vibrational, rotation and translational partition function for gaseous species. Adsorption and desorption are taken into account only for stable species (H_2, CO_2, HCOOH, HCHO, CH_3OH). Calculations were carried out for temperatures 150, 200, 250, and 300 °C that roughly cover the industrially important temperature range.

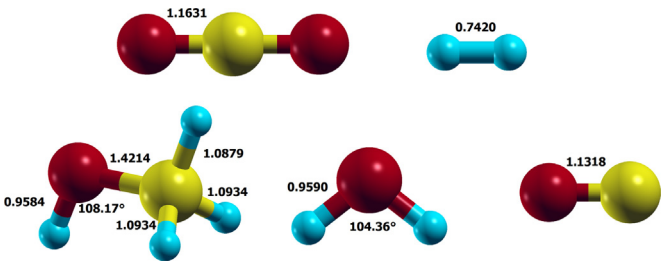

Fig. 1. Optimised geometries of reactants (CO_2, H_2) and products (CH_3OH, H_2O, CO) from CCSD(T)/aug-cc-pVQZ calculations. All digits shown are within the margin of error.

2.3. Catalyst synthesis, characterisation and catalytic testing

The synthesised Cu/Zn/Al catalyst (Cu:Zn:Al=50:30:20) was prepared by a co-precipitation method at a constant pH (~8) and a constant temperature (60 °C), as described in [36]. The synthesised catalyst was characterised by BET (Brunauer–Emmett–Teller) surface area measurement and pore volume studies, powder X-ray diffraction (XRD), scanning electron microscopy (SEM), energy-dispersive X-ray spectroscopy (EDXS), and scanning transmission electron microscopy (TEM). The activity evaluation of the catalyst for CO_2 hydrogenation to methanol was carried out in a continuous-flow, high pressure, fixed-bed reactor. The catalytic testing was done at a GHSV of 2000 h^{-1} with a mixture of CO_2 and H_2 gases (CO_2:H_2=1:3). The pressure of the reactor was kept constant at 20 bar with varying the temperatures from 200 to 400 °C.

The catalyst synthesised in such a way closely mimics the commercially used catalysts in terms of active phase. However, by synthesising the catalyst ourselves instead of analysing a commercial one, we have avoided the unwanted effects of inert components (*e.g.* binders, mechanical stabilisers) on the characterisation. For a more detailed description of catalyst characterisation and catalytic testing, refer to the Supporting information.

3. Results

3.1. Reaction thermodynamics

Hydrogenation of carbon dioxide to methanol is an exothermic reaction with experimentally determined enthalpy change $\Delta H_{298\,K}$ = −48.98 kJ/mol [37]. As two molecules of products form from four molecules of reactants, low temperature and high pressure favour the production of methanol. Consequently, a compromise must be struck between high temperatures, which increase the reaction rate, and low temperatures, which increase the conversion. This obstacle is overcome with reactors using recycle, which can achieve almost 100% conversion. At high temperatures, however, the reverse water–gas shift (RWGS) reaction becomes dominant as it is endothermic and pressure-independent. The experimentally determined enthalpy change for RWGS is $\Delta H_{298\,K}$ = +41.16 kJ/mol [37].

In Tables 1 and 2, thermodynamics of the two reactions at different industrially relevant conditions is listed, as calculated with CCSD(T)/aug-cc-pVQZ. Fig. 1 shows the minimum energy geometry for reactants and products.

Table 1
Reaction enthalpy, entropy, Gibbs free energy and equilibrium constants from CCSD(T)/aug-cc-pVQZ for $CO_2 + 3\,H_2 \rightarrow CH_3OH + H_2O$ at different temperatures and pressures, relevant for industrial operations.

	ΔH (kJ mol^{-1})	ΔS (J mol^{-1} K^{-1})					ΔG (kJ mol^{-1})					K_p				
T (°C) / p (bar)	All	1	20	40	60	100	1	20	40	60	100	1	20	40	60	100
25	−51.61	−171.53	−121.71	−110.19	−103.44	−94.65	−0.47	−15.33	−18.76	−20.77	−23.30	1.21E+00	4.85E+02	1.94E+03	4.36E+03	1.21E+04
150	−57.00	−186.68	−136.87	−125.34	−118.60	−110.10	+12.78	−5.81	−10.11	−12.62	−15.79	1.93E−03	7.71E−01	3.09E+00	6.94E+00	1.93E+01
200	−58.92	−190.98	−141.15	−129.64	−122.89	−114.40	+31.44	+7.86	+2.42	−0.78	−4.79	3.38E−04	1.35E−01	5.41E−01	1.22E+00	3.38E+00
250	−60.69	−194.54	−144.72	−133.18	−126.45	−117.95	+41.08	+15.02	+8.98	+5.46	+1.01	7.91E−05	3.16E−02	1.27E−01	2.85E−01	7.92E−01
300	−62.30	−197.47	−147.66	−136.14	−129.39	−120.90	+50.88	+22.33	+15.73	+11.86	+6.99	2.31E−05	9.22E−03	3.69E−02	8.30E−02	2.30E−01

Table 2
Reaction enthalpy, entropy, Gibbs free energy and equilibrium constants from CCSD(T)/aug-cc-pVQZ for $CO_2 + H_2 \rightarrow CO + H_2O$ at different temperatures, relevant for industrial operations. Note that this reaction is pressure-independent.

T (°C)	ΔH (kJ mol^{-1})	ΔS (J mol^{-1} K^{-1})	ΔG (kJ mol^{-1})	K_p
25	+37.71	+48.00	+23.40	7.96E−05
150	+36.99	+46.04	+17.51	6.89E−03
200	+36.59	+45.15	+15.23	5.04E−02
250	+36.15	+44.26	+13.00	1.88E−01
300	+35.69	+43.40	+10.81	3.10E−01

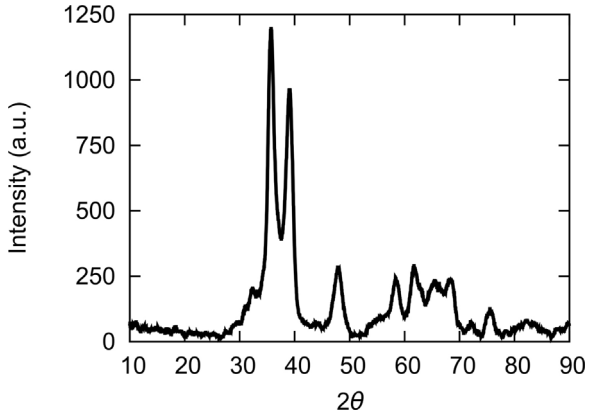

Fig. 2. Powder pattern X-ray diffraction of the catalyst after calcination prior to reduction with hydrogen.

3.2. Structure determination

DFT studies usually focus on simple mono- or bimetallic surfaces. To model the catalyst as realistically as possible, several experimental characterisation techniques were used to elucidate the structure of the synthesised CuZnAl catalyst well enough. The results are summarised in Table 3. For more detailed information, additional results, and comments, the reader is referred to the Supporting information (Fig. S2).

The synthesised catalyst was characterised after calcination but before final reduction, which is essential for the activity of the catalyst and is performed immediately prior to reaction in the reactor under the hydrogen flow. Powder XRD shows (Fig. 2) the characteristic peaks for the Cu and spinel species such as $CuAl_2O_4$ (JCPDS 01-1153) and $ZnAl_2O_4$ (JCPDS 05-0669) at 2θ of 32°, 35°, 39° and 48°. It is difficult to distinguish between $CuAl_2O_4$ and $ZnAl_2O_4$, as they have almost identical diffraction patterns [40]. The formation of $ZnAl_2O_4$ spinel species can be assumed on the account of the disappearance of some characteristic peaks of ZnO upon calcination (not shown here) [41]. The low intensity of peaks for Cu, apparently accompanied with peaks of high intensity for $CuAl_2O_4$ and $ZnAl_2O_4$, suggests that after calcination a complete decomposition of the hydrotalcite-like precursor occurred and the increased particle size of $CuAl_2O_4$ and $ZnAl_2O_4$ is responsible for the dispersion of copper [41,42]. Broadening of the peaks indicates small crystallite sizes in the range of 10 nm [38,39]. None of the alumina peaks were observed in the XRD patterns, which indicated their amorphous or highly disordered state.

The SEM and TEM micrographs (see Supporting information) of the prepared catalyst support the XRD results. Specifically, no extensive agglomeration of CuO or alkaline earth oxide was observed. Moreover, the isolated Cu^{2+} species can strongly interact with alumina to the extent that can result in the formation of copper aluminate on the surface. Nonetheless, this phase cannot be singled out by XRD.

Table 3
Particulate properties of Cu–Zn–Al catalyst prepared *via* co-precipitation.

Theoretical composition (Cu:Zn:Al)	Surface area (m^2/g)	Cu metal dispersion (%)	Cu metallic surface area (m^2/g)	Crystallite size (nm)	H_2 chemisorbed (μmol/g)	Basicity (μmol/g)
50/30/20	96	28	48	14	31	22

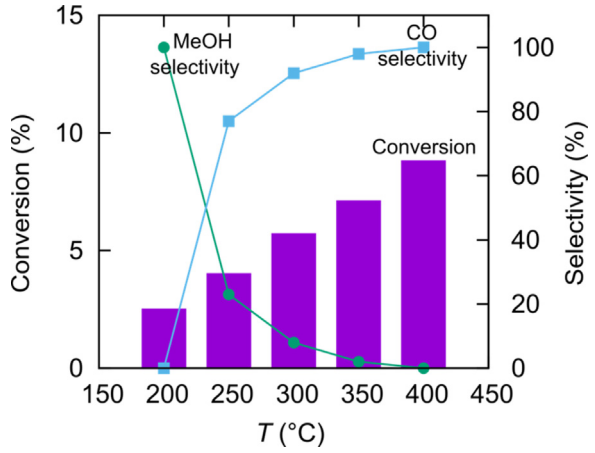

Fig. 3. Effect of temperature on CO_2 conversion and methanol (MeOH) selectivity over Cu/Zn/Al catalyst (CO_2:H_2 ratio 1:3, GHSV of 2000 h^{-1} and pressure = 20 bar).

3.3. Catalytic performance

To ensure that the synthesised and characterised catalyst is indeed capable of CO_2 conversion into methanol, some preliminary catalytic testing was performed. The results are summarised in Fig. 3. Methanol, carbon monoxide and water are the main products under the reaction conditions. There are no traces of methane and higher hydrocarbons detected. The catalyst showed low conversion and high methanol selectivity at lower temperatures, *i.e.* 200 and 250 °C. At higher temperatures, the conversion increased at the expense of methanol selectivity.

These results justify the choice of the catalyst for modelling. As this study aims to computationally establish the most probable pathway for production of methanol and identify the bottlenecks, we are interested in the catalytic activity of the catalyst investigated insofar that the methanol is produced in noticeable amounts.

3.4. Catalyst structure modelling

Based on the experimental results and accounting for the synergistic effects of Zn, Cu and alumina, the catalyst was modelled as $ZnAl_2O_4$ in a spinel structure with active cluster Cu_3Zn_3 on its 110 Miller plane. The namesake of spinel structure is the mineral $MgAl_2O_4$, which crystallises in a cubic unit cell in the *Fd3m* space group. There are eight formula units of $ZnAl_2O_4$ per unit cell, as shown in Fig. 4. Atomic positions in an ideal spinel structure [43] are shown in Table 4. After the relaxation of the $ZnAl_2O_4$ crystal, the parameter u in our model was determined to be 0.390 and the lattice parameter was 7.951 Å. As the catalyst is only active after the reduction in hydrogen environment, the surface was Zn-terminated and had Cu_3Zn_3 cluster deposited in the most favourable position (see Fig. 5). In this manner, we mimic the interface between the Cu^0, Cu(I), ZnO and support as the active site.

It is important to note the non-trivial relationship between the element ratio used for catalyst preparation (Cu:Zn:Al=50:30:20) and the model used in DFT calculations. After the hydrogenation of catalyst, which is needed for activity, clusters of Cu^0 and Cu(I) interspersed with ZnO are formed, having substantially different composition than bulk. Their interface plays the most crucial role in the catalyst activity. As the active site in the calculation spans at most a few atoms, the Cu_3Zn_3 cluster on the spinel-type support is deemed adequate for this study. In reality, the catalyst displays many surfaces with different Miller indices and several interfaces.

Table 4
Fractional coordinates of lattice sites in a cubic unit cell for ideal spinel structure.

Lattice site	Point symmetry	Ideal positions in AB_2X_4
A (Zn^{2+})	$\bar{4}3m$	(0,0,0) (0.25,0.25,0.25)
B (Al^{3+})	$\bar{3}m$	(0.625,0.625,0.625) (0.625,0.875,0.875) (0.875,0.625,0.875) (0.875,0.875,0.625)
X (O^{2-})	$3m$	(u,u,u) u = 0.375 (u,$\bar{u}$,$\bar{u}$) ($\bar{u}$,u,$\bar{u}$) ($\bar{u}$,$\bar{u}$,u) (¼ −u, ¼−u, ¼−u) (¼+u, ¼+u, ¼−u) (¼+u, ¼−u, ¼+u) (¼ −u, ¼+u, ¼+u)

3.5. Adsorption

Adsorption energy of a species is calculated as shown in the Section 2. Negative sign of ZPE-corrected adsorption energies (E_{ads}^{ZPE}) signifies that adsorption is an exothermic process in all instances. This also follows from a simple thermodynamic analysis: degrees of freedom are lost during the adsorption, which in turn decreases entropy of the system. For adsorption to be spontaneous, it has to be exothermic (as $\Delta G = \Delta H - T\Delta S < 0$ must hold true). Adsorption is also important for studying catalyst poisoning – adsorbates with particularly high adsorption energies and unfavourable reaction barriers are known to poison the catalyst.

In this paragraph, we list all reactants, intermediates and products, which were considered within the reaction pathway framework. Most adsorbates have various adsorption models. For instance, HCOO can adsorb with either oxygen atoms over copper atoms or one oxygen atom over copper atom and the other oxygen atom over zinc atom. For all species, the most stable adsorption models are reported. Adsorption modes that do not follow from the reaction network are not considered. Detailed numerical data are presented in Table 5, while Fig. 6 graphically depicts the optimised adsorption geometries.

Carbon dioxide interacts only weakly with the catalyst as its adsorption energy equals −0.24 eV. Moreover, this interaction is non-specific, as it remains roughly unchanged regardless of the carbon dioxide position, provided that it lies flat above the catalyst surface. This is indicative of the physisorption and Eley–Rideal mechanism. Dissociative adsorption of hydrogen molecule is energetically favourable with hydrogen atom adsorption energy −3.00 eV. Hydrogen atom prefers to bind to the bridge site between copper and zinc atom.

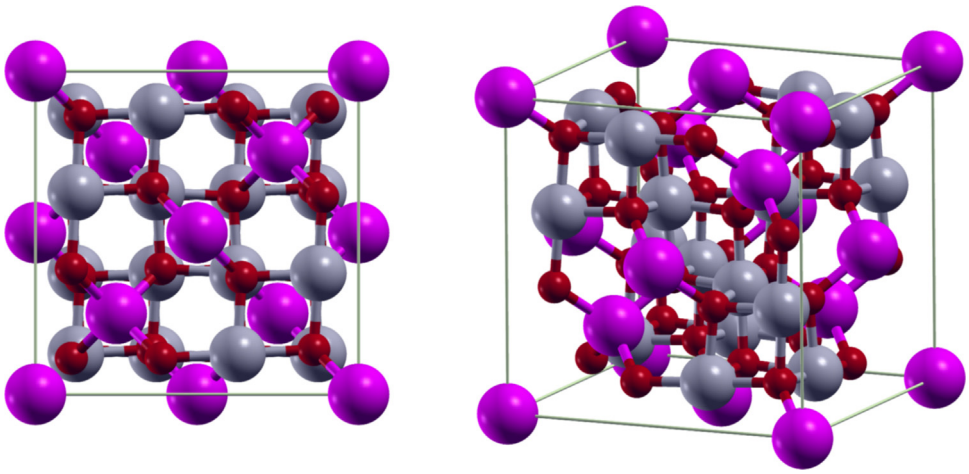

Fig. 4. Optimised conventional (non-primitive) unit cell of spinel-type $ZnAl_2O_4$. Zn atoms are shown in purple, Al in grey, O in red. Left: top view, right: perspective (note that the op five Zn atoms lie on the same plane). (For interpretation of the references to colour in this figure legend, the reader is referred to the web version of this article.)

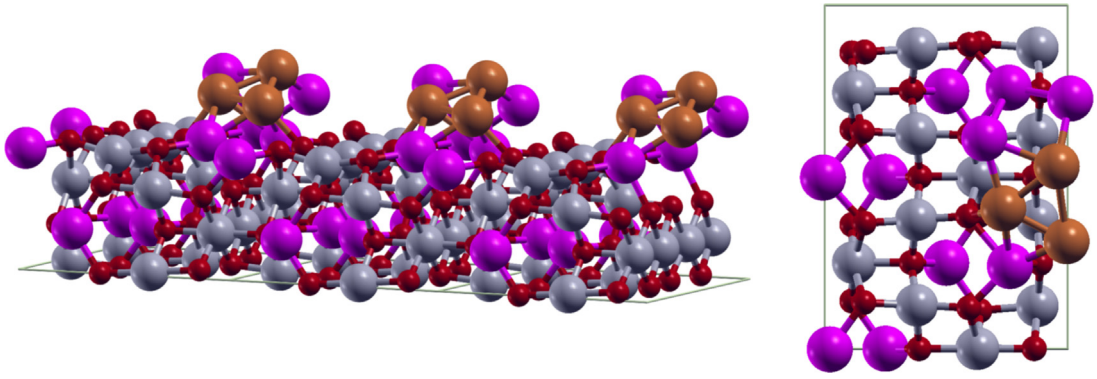

Fig. 5. Active cluster Cu_3Zn_3 on top of 110 plane of $ZnAl_2O_4$ support. Left: three unit cells in perspective, right: top view of a single unit cell. Cu in bronze, other colours as in Fig. 4. (For interpretation of the references to colour in this figure legend, the reader is referred to the web version of this article.)

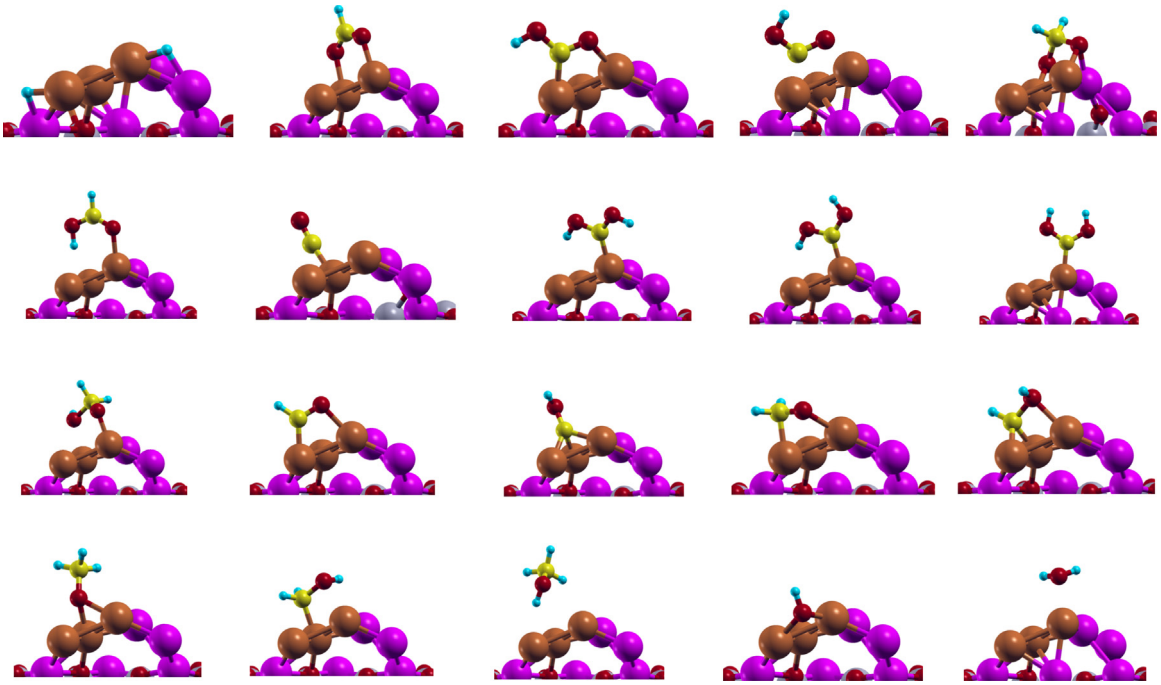

Fig. 6. Minimum energy geometries of stable intermediates on the catalyst active site cluster, shown in side view. From top left: H, HCOO, t-HOCO, c-HOCO, H_2COO, HCOOH, CO, t,t-HOCOH, c,t-HOCOH, c,c-HOCOH, H_2COOH, HCO, COH, CH_2O, HCOH, H_3CO, H_2COH, CH_3OH, OH, H_2O.

Table 5
Calculated geometry and energetics of reaction intermediates on the catalyst. E_{ads} and E_{ads}^{ZPE} are binding energy and zero-point-energy corrected binding energies for the optimised intermediate structure, respectively.

Adsorbate	Site	E_{ads} (eV)	E_{ads}^{ZPE} (eV)	Bond length (Å)	Angle (Å)
H	Bridge over Cu–Zn	−3.05	−3.00	n/a	n/a
CO_2	Non-specific	−0.26	−0.24	C–O: 1.18	∠OCO: 178
HCOO	Bridge over Cu–Cu	−3.23	−3.15	C–O: 1.28	∠OCO: 128
				C–H: 1.11	∠OCH: 116
t-HOCO	Bridge over Cu–Cu	−2.10	−2.02	O–C: 1.27	∠OCO: 113
				C–O: 1.37	∠COH: 106
				O–H: 0.98	
c-HOCO	Bridge over Cu–Cu	−2.22	−2.14	O–C: 1.28	∠OCO: 115
				C–O: 1.36	∠COH: 108
				O–H: 0.99	
H_2COO	3-fold hollow between Cu–Cu–Zn	−4.28	−4.11	O–C: 1.44	∠OCO: 109
				C–H: 1.11	∠OCH: 110
					∠HCH: 111
HCOOH	Atop of Cu	−0.71	−0.66	H–O: 1.04	∠HOC: 110
				O–C: 1.33	∠OCO: 127
				C–H: 1.11	∠OCH: 122
				C–O: 1.24	
CO	Atop of Cu	−1.17	−1.07	C–O: 1.16	n/a
t,t-HOCOH	Atop of Cu	−1.81	−1.75	H–O: 0.99	∠HOC: 105
				C–O: 1.34	∠OCO: 108
c,t-HOCOH	Atop of Cu	−1.80	−1.71	H–O: 0.99	∠HOC: 105
				O–C: 1.34	∠OCO: 108
				C–O: 1.33	∠HOC: 112
				O–H: 1.02	∠OCO: 115
c,c-HOCOH	Atop of Cu	−1.20	−1.08	H–O: 1.01	∠HOC: 113
				C–O: 1.33	∠OCO: 116
H_2COOH	3-fold hollow between Cu–Cu–Zn	−3.00	−2.90	H–O: 0.99	∠HOC: 105
				(H)O–C: 1.48	∠OCO: 114
				C–H: 1.11	∠HCH: 111
				C–O: 1.39	∠OCH: 109
HCO	Atop of Cu	−2.91	−2.88	H–C: 1.13	∠HCO: 115
				C–O: 1.26	
COH	3-fold hollow between Cu–Cu–Cu	−4.05	−3.99	H–O: 0.98	∠COH: 109
				O–C: 1.38	
CH_2O	Bridge over Cu–Cu	−0.84	−0.81	H–C: 1.11	∠HCO: 117
				C–O: 1.33	∠HCH: 115
HCOH	3-fold hollow between Cu–Cu–Cu	−2.78	−2.73	H–C: 1.11	∠HCO: 110
				C–O: 1.47	∠OCH: 108
				O–H: 0.97	
H_3CO	3-fold hollow between Cu–Cu–Cu	−1.94	−1.83	H–C: 1.10	∠OCH: 111
				C–O: 1.44	∠HCH: 109
H_2COH	Bridge over Cu–Cu	−1.44	−1.38	H–O: 0.98	∠HOC: 109
				O–C: 1.49	∠OCH: 109
				C–H: 1.10	∠HCH: 110
CH_3OH	Atop of Cu	−0.44	−0.41	H–O: 0.99	∠HOC: 106
				O–C: 1.44	∠OCH: 106
				C–H: 1.10	∠HCH: 109
OH	Bridge over Cu–Cu	−3.55	−3.41	O–H: 0.97	n/a
H_2O	Atop of Cu	−0.48	−0.46	O–H: 0.98	∠HOH: 104

In contrast to both monodentate and bidentate configurations on pure copper surfaces [10], formate species (HCOO) was found to bind only as a bidentate species. When in a bridge site over two copper atoms, its adsorption energy is −3.15 eV. Hydroxycarbonyl intermediate (HOCO) can be found in two configurations, either *trans* or *cis* with respect to C–O bond. It adsorbs marginally more strongly in *cis* configuration (−2.14 *vs* −2.02 eV).

H_2COO, although experimentally not confirmed in the methanol synthesis from carbon dioxide, is assumed to play a crucial role in the formation of methanol [44]. It is formed *via* direct hydrogenation of formate and is strongly bound to the surface (−4.11 eV) with carbon atom lying above 3-fold hollow and oxygen atoms occupying Cu–Zn bridge sites. Formic acid (HCOOH) binds on top site over a copper atom with its oxygen more strongly (−0.71 eV) than on pure copper [45]. Hydroxyl hydrogen points towards the catalyst surface. Carbon monoxide (CO) strongly binds on top of Cu with carbon atom (−1.07 eV).

Dihydroxycarbene (HOCOH), which can form through hydrogenation of hydroxycarbonyl, exists in three different isomers due to *cis* and *trans* isomerism of substituents on either side of C–O bond (*t–t*, *c–t*, and *c–c*). Two of them have been experimentally confirmed using infrared spectroscopy [46]. They all bind to the top site of Cu with adsorption energies of −1.75, −1.71 and −1.08 eV, respectively. As on pure copper [10], the *t,t* isomer with hydrogen atoms pointing towards the catalytic surface is the most stable configuration, although further reactions proceed from *c,c* isomer.

Hydroxymethoxy (H_2COOH) is an intermediate that can form either H_2COO or HCOOH. It binds quite strongly (−2.90 eV) to the bridge site between Cu–Zn with oxygen atom and bridge site between Cu–Cu with hydroxyl oxygen, while the carbon atom resides above 3-fold hollow site. Formyl (HCO) binds on top site on Cu (−2.88 eV), while hydroxymethylidyne (COH) binds with carbon atom on 3-fold hollow site (−3.99 eV).

Formaldehyde (CH_2O) adopts a planar position above the Cu–Cu bridge and binds with oxygen atom to one Cu and carbon atom to another Cu (−0.81 eV). This rather strong adsorption energy for a stable molecule is congruent with a fact that formaldehyde binds weakly to pure copper surface but rather strongly to an

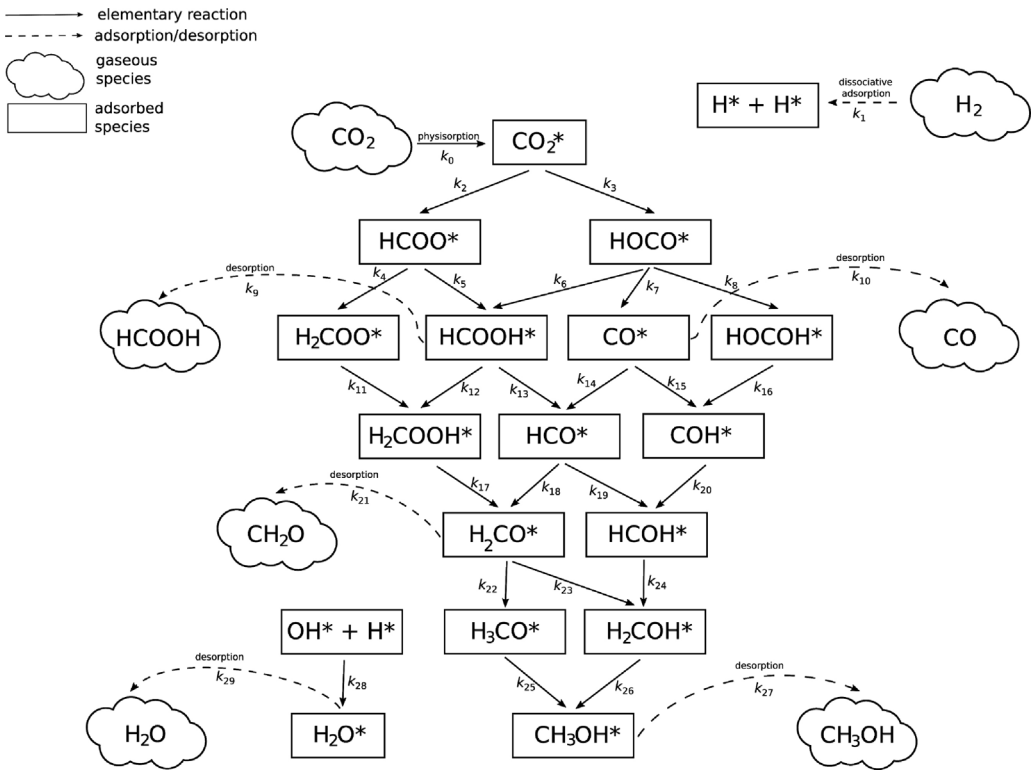

Fig. 7. Pathway of all possible elementary reaction steps investigated in this work. Note that H* and OH* species are omitted for the sake of clarity and all reactions are in principle reversible.

active cluster of copper on ZnO support [47]. Hydroxymethylene (HCOH) is an alternative intermediate that can be formed from either COH or HCO. It adopts a *cis* configuration of hydrogen atoms around the C–O bond and binds to the 3-fold hollow site with carbon (−2.73 eV). Methoxy (H_3CO) binds in an upright position with oxygen atom to the 3-fold hollow site (−1.83 eV). Hydroxymethyl (H_2COH) binds in a planar orientation with over Cu–Cu bridge (−1.38 eV).

Methanol (CH_3OH) only weakly interacts with the catalyst surface. It binds with the oxygen atom to the surface above the Cu top site. Hydroxyl (OH) coordinates to bridge sites, either over Cu–Cu (−3.41 eV) or Cu–Zn (−4.01 eV). In all instances, it binds with oxygen atom. Water binds to the top site over Cu with oxygen (−0.46 eV).

3.6. Elementary reaction steps

As shown in Fig. 7, there are several pathways leading to formation of methanol. In addition to well-studied formate and RWGS mechanisms, there are also side pathways and elementary steps linking the two mechanisms. We exhaustively studied possible elementary reaction steps in order to thoroughly understand a complex reaction network and identify the main reaction pathway. Calculated reaction energies, activation barriers, equilibrium constants, and reaction rates for all elementary reaction steps at various temperatures are listed in Table 6.

3.6.1. Carbon dioxide physisorption

CO_2 interaction with the catalyst is weak and not dependent on its position. It changes monotonically from zero at infinite separation to −0.24 eV, being indicative of non-specific van der Waals attraction. This weak physisorption is in agreement with CO_2 calculations on pure Cu(111) [10] and Cu_2O(111) [48]. Geometry of the CO_2 remains unperturbed upon physisorption.

3.6.2. Dissociative hydrogen adsorption

Hydrogen adsorbs dissociatively on many metallic catalysts. Our results show that it adsorbs on bridge sites between the Cu and Zn atoms, while most reactions take place at the Cu active site (*vide infra*). This agrees well with the experimental fact that hydrogen spill-over is an important step in the catalytic hydrogenation of CO_2. Energy of reaction H_2 (g) → 2 H* is calculated to be −0.68 eV with the activation barrier 0.47 eV.

3.6.3. Formate reaction pathway

Formate reaction route begins with hydrogenation of CO_2 to HCOO and proceeds *via* H_2COO, H_2COOH, H_2CO and H_3CO. HCOO can be formed from either weakly physisorbed CO_2 or directly from gaseous CO_2 (Eley–Rideal mechanism). In the first instance, activation barrier is 1.07 eV and energy of reaction is +0.10 eV. When gaseous CO_2 reacts, activation barrier is 0.83 eV and energy of reaction is −0.14 eV. In either case, HCOO is bound through two Cu–O bonds (2.05 Å). Monodentate HCOO species, although observed on some metals, is not stable on this catalyst.

HCOO can react to either H_2COO or HCOOH. Activation barrier for the formation of H_2COO is 1.22 eV and the reaction energy is +0.45 eV, which is very similar to reaction on pure Cu(111) [10]. Reaction to HCOOH appears to be kinetically more accessible with activation barrier 0.78 eV. However, reaction energy +0.61 eV means that the reverse reaction has a very low activation barrier of 0.17 eV. Additionally, HCOO could also decompose into HCO and O. Preliminary calculations have shown the activation barrier of this reaction to exceed 2 eV, making it kinetically irrelevant.

H_2COO is further hydrogenated to H_2COOH. Cleavage of C–O bond to yield H_2CO and O is kinetically prohibited with activation energy of 1.8 eV. Formation of H_2COOH is endothermic (+0.45 eV) and relatively slow with an activation barrier of 1.19 eV. Hydrogenation of HCOOH to H_2COOH has a lower reaction barrier (0.94 eV) and is slightly more endothermic (+0.56 eV). HCOOH can

Table 6
Calculated reaction energies (ΔE), activation barriers (E_A), equilibrium constants (K), and reaction rates constants (k_{fwd}) for all elementary reaction steps at various temperatures (150, 200, 250 and 300 °C). Note that the reaction rates constants have the same unit (s^{-1}) regardless of the molecularity, as reaction rate on the catalyst is properly defined as $k_{fwd}C_{AS}\prod_{i=1}^{n}\theta_i$, where c_{AS} stands for concentration of active sites and θ_i for surface coverage of reactant i on the catalyst.

Step	Reaction	Constant	T (°C) 150	200	250	300
0	CO_2 (g) → CO_2*	K	1.57E−06	5.31E−07	2.14E−07	9.80E−08
	ΔE = −0.24 eV	k_0 [s^{-1} bar^{-1}]	7.39E+09	6.99E+09	6.64E+09	6.35E+09
1	H_2 (g) → 2 H*	K	1.06E+12	3.12E+10	1.70E+09	1.47E+08
	ΔE = −1.08 eV, E_A = 0.47 eV	k_0 s^{-1} bar^{-1}]	3.46E+10	3.28E+10	3.12E+10	2.98E+10
2	CO_2* + H* → HCOO*	K	6.44E−02	8.36E−02	1.03E−01	1.21E−01
	ΔE = +0.10 eV, E_A = 1.07 eV	k_{fwd} [s^{-1}]	2.44E+00	6.18E+01	8.52E+02	7.49E+03
3	CO_2* + H* → t-HOCO*	K	2.65E−11	3.31E−10	2.55E−09	1.37E−08
	ΔE = +0.88 eV, E_A = 2.23 eV	k_{fwd} [s^{-1}]	1.06E−13	7.93E−11	1.70E−08	1.45E−06
4	HCOO* + H* → H_2COO*	K	3.44E−06	1.24E−05	3.49E−05	8.16E−05
	ΔE = +0.45 eV, E_A = 1.22 eV	k_{fwd} [s^{-1}]	3.54E−02	1.37E+00	2.68E+01	3.15E+02
5	HCOO* + H* → HCOOH*	K	2.21E−07	1.31E−06	5.53E−06	1.80E−05
	ΔE = +0.61 eV, E_A = 0.78 eV	k_{fwd} [s^{-1}]	2.34E+04	2.68E+05	1.95E+06	1.02E+07
6	t-HOCO* + H* → HCOOH	K	2.71E+04	1.28E+04	6.96E+03	4.19E+03
	ΔE = −0.28 eV, E_A = 0.68 eV	k_{fwd} [s^{-1}]	9.06E+05	8.71E+06	5.54E+07	2.59E+08
7a	t-HOCO* → c-HOCO*	K	1.63E+01	1.10E+01	7.98E+00	6.12E+00
	ΔE = −0.13 eV, E_A = 0.44 eV	k_{fwd} [s^{-1}]	3.25E+07	1.35E+08	4.35E+08	1.15E+09
7b	c-HOCO* → OH* + CO*	K	2.36E+05	7.80E+04	3.22E+04	1.56E+04
	ΔE = −0.42 eV, E_A = 0.98 eV	k_{fwd} [s^{-1}]	1.86E+01	3.76E+02	4.36E+03	3.34E+04
8a	t-HOCO* + H* → t,t-HOCOH*	K	8.26E−08	5.96E−07	2.94E−06	1.10E−05
	ΔE = +0.66 eV, E_A = 1.90 eV	k_{fwd} [s^{-1}]	2.19E−09	7.02E−07	7.60E−05	3.68E−03
8b	t,t-HOCOH* → c,t-HOCOH*	K	3.88E+00	3.83E+00	3.78E+00	3.75E+00
	ΔE = −0.01 eV, E_A = 0.59 eV	k_{fwd} [s^{-1}]	2.06E+06	1.37E+07	6.43E+07	2.34E+08
8c	c,t-HOCOH* → c,c-HOCOH*	K	1.98E−08	1.21E−07	5.22E−07	1.75E−06
	ΔE = +0.62 eV, E_A = 0.87 eV	k_{fwd} [s^{-1}]	6.74E+02	9.87E+03	8.80E+04	5.42E+05
9	HCOOH* → HCOOH (g)	K	3.56E+01	4.47E+02	4.01E+03	2.41E+04
	ΔE = +0.66 eV	k_{fwd} [s^{-1}]	2.57E+11	3.24E+12	2.60E+13	1.50E+15
10	CO* → CO (g)	K	1.29E−05	4.41E−04	7.96E−03	8.94E−02
	ΔE = +1.07 eV	k_{fwd} [s^{-1}]	1.19E+05	3.86E+06	6.63E+07	7.11E+08
11	H_2COO* + H* → H_2COOH*	K	3.31E−06	1.22E−05	3.47E−05	8.21E−05
	ΔE = +0.45 eV, E_A = 1.19 eV	k_{fwd} [s^{-1}]	8.65E−02	3.14E+00	5.81E+01	6.51E+02
12	HCOOH* + H* → H_2COOH*	K	3.09E−08	1.46E−07	5.09E−07	1.42E−06
	ΔE = +0.56 eV, E_A = 0.94 eV	k_{fwd} [s^{-1}]	2.69E+01	4.77E+02	4.96E+03	3.48E+04
13	HCOOH* → HCO* + OH*	K	2.74E−15	8.76E−14	1.46E−12	1.50E−11
	ΔE = +1.19 eV, E_A = 1.49 eV	k_{fwd} [s^{-1}]	2.31E−04	2.42E−02	1.07E+00	2.49E+01
14	CO* + H* → HCO*	K	3.58E−13	8.88E−12	1.19E−10	1.01E−09
	ΔE = +1.10 eV, E_A = 1.54 eV	k_{fwd} [s^{-1}]	9.19E−06	9.60E−04	4.18E−02	9.52E−01
15	CO* + H* → COH*	K	5.86E−24	1.55E−21	1.42E−19	5.86E−18
	ΔE = +1.94 eV, E_A = 2.79 eV	k_{fwd} [s^{-1}]	4.04E−21	1.43E−17	1.07E−14	2.55E−12
16	c,c-HOCOH* → COH* + OH*	K	2.41E+09	2.70E+08	4.64E+07	1.09E+07
	ΔE = −0.78 eV, E_A = 1.88 eV	k_{fwd} [s^{-1}]	7.67E−10	2.15E−07	2.09E−05	9.30E−04
17	H_2COOH* → H_2CO* + OH*	K	2.59E+00	2.52E+00	2.48E+00	2.48E+00
	ΔE = −0.03 eV, E_A = 0.58 eV	k_{fwd} [s^{-1}]	2.26E+07	1.68E+08	8.73E+08	3.46E+09
18	HCO* + H* → H_2CO*	K	1.59E+06	3.25E+05	8.96E+04	3.08E+04
	ΔE = −0.54 eV, E_A = 0.70 eV	k_{fwd} [s^{-1}]	7.87E+04	7.22E+05	4.40E+06	1.98E+07
19	HCO* + H* → HCOH*	K	1.03E−14	2.77E−13	4.01E−12	3.64E−11
	ΔE = +1.14 eV, E_A = 1.83 eV	k_{fwd} [s^{-1}]	1.07E−08	2.64E−06	2.32E−04	9.48E−03
20	COH* + H* → HCOH*	K	6.65E+07	1.12E+07	2.66E+06	8.06E+05
	ΔE = −0.63 eV, E_A = 0.31 eV	k_{fwd} [s^{-1}]	3.00E+09	8.74E+09	2.10E+10	4.39E+10
21	H_2CO* → CH_2O (g)	K	6.68E−02	1.21E+00	1.31E+01	9.96E+01
	ΔE = +0.81 eV	k_{fwd} [s^{-1}]	5.98E+08	1.02E+10	1.05E+11	7.40E+11
22	H_2CO* + H* → H_3CO*	K	1.00E−08	6.94E−08	3.30E−07	1.19E−06
	ΔE = +0.68 eV, E_A = 0.72 eV	k_{fwd} [s^{-1}]	3.13E+05	3.09E+06	2.00E+07	9.44E+07
23	H_2CO* + H* → H_2COH*	K	7.08E−13	1.21E−11	1.20E−10	7.95E−10
	ΔE = +1.00 eV, E_A = 1.81 eV	k_{fwd} [s^{-1}]	4.57E−09	1.02E−06	8.20E−05	3.10E−03
24	HCOH + H* → H_2COH*	K	4.59E−03	8.33E−03	1.34E−02	1.98E−02
	ΔE = +0.21 eV, E_A = 0.63 eV	k_{fwd} [s^{-1}]	2.61E+05	1.82E+06	8.77E+06	3.24E+07
25	H_3CO* + H* → CH_3OH*	K	6.43E+02	3.73E+02	2.39E+02	1.65E+02
	ΔE = −0.20 eV, E_A = 0.69 eV	k_{fwd} [s^{-1}]	4.45E+05	4.09E+06	2.49E+07	1.12E+08
26	H_2COH*+ H* → CH_3OH*	K	1.01E−07	8.32E−07	4.56E−06	1.85E−05
	ΔE = +0.64 eV, E_A = 0.71 eV	k_{fwd} [s^{-1}]	7.69E+05	6.12E+06	3.33E+07	1.37E+08
27	CH_3OH* → CH_3OH (g)	K	7.20E+05	2.54E+06	7.20E+06	1.73E+07
	ΔE = +0.41 eV	k_{fwd} [s^{-1}]	6.23E+15	2.08E+16	5.60E+16	1.28E+17
28	OH* + H* → H_2O*	K	1.90E−04	5.87E−04	1.46E−03	3.11E−03
	ΔE = +0.36 eV, E_A = 1.25 eV	k_{fwd} [s^{-1}]	1.96E−02	8.83E−01	1.95E+01	2.53E+02
29	H_2O*→ H_2O (g)	K	1.31E+02	8.04E+02	3.62E+03	1.30E+04
	ΔE = +0.46 eV	k_{fwd} [s^{-1}]	1.52E+12	8.77E+12	3.76E+13	1.29E+14

also desorb, as it is only moderately bound to the surface *via* one Cu–O bond (0.66 eV).

H_2COOH readily decomposes into H_2CO and OH with activation barrier 0.58 eV. This step is slightly exothermic (−0.03 eV). Formaldehyde that is formed is strongly bound (−0.81 eV) to the catalyst and does not desorb noticeably. H_2COOH is bound to the catalyst with two Cu–O bonds (1.89 and 2.23 Å for Cu–O and Cu–O(H), respectively).

Formaldehyde can convert into CH_3O or CH_2OH. Reaction barrier for formation of CH_3O is 0.72 eV and energy of reaction is 0.68 eV. This means that the equilibrium between both species is quickly established. Any CH_3O that is formed, however, either decomposes back into CH_2O or reacts to methanol with reaction barrier 0.69 eV in an exothermic step (−0.20 eV). Alternative hydrogenation of H_2CO to H_2COH is unlikely due to high reaction barrier (1.81 eV). Ultimately, CH_3OH desorbs (+0.41 eV).

3.6.4. RWGS reaction pathway

RWGS route is an alternative route through which hydrogenation of CO_2 can proceed if the first hydrogen atom attaches to oxygen. As carbon monoxide is one of the main products of this route, it is generally undesirable, although some metals favour the formation of methanol *via* this route [14]. Our results show the first step in this route to be very unlikely with activation barrier 2.23 eV and energy of reaction +0.88 eV. Nevertheless, should this reaction take place, HOCO would form in *trans* conformer, which is bound with Cu–C bond (1.92 Å) and with hydrogen atom pointing towards the catalyst surface.

It can then either be hydrogenated into HCOOH in an exothermic step (−0.28 eV) with a moderate reaction barrier of 0.68 eV or it can isomerise into *cis*-HOCO with reaction barrier of 0.44 eV. HCOOH links RWGS route with the formate route, as it can converts into H_2COOH (*vide supra*) or decomposes into HCO and OH. The latter possibility is extremely costly with reaction energy +1.19 eV and the barrier of 1.49 eV is not realistically accessible. The more favourable route would be for *cis*-HOCO to decompose into OH and CO in an exothermic step (−0.42 eV) with reaction barrier 0.98 eV.

CO remains strongly bound to the surface (−1.07 eV) and can be hydrogenated into HCO, although the reaction barrier is somewhat large with 1.54 eV. HCO is finally hydrogenated into H_2CO with reaction barrier of 0.70 eV in an exothermic reaction (−0.54 eV). Thenceforth, this route merges with the formate pathway.

3.6.5. Side pathways

We also investigated some elementary reaction steps that are less frequently reported or are deemed to not be relevant for the formation of methanol. They are included here for the sake of completeness.

Firstly, *trans*-HOCO could convert into *trans,trans*-HOCOH, which is bound *via* single Cu–C bond (1.92 Å) and has both hydrogen atoms pointing towards the catalyst surface. The reaction barrier for this step is 1.90 eV, which is too large for the reaction to take place. It would then have to convert into *cis,trans*-HOCOH and ultimately *cis,cis*-HOCOH with barriers of 0.59 and 0.87 eV, respectively. Only *cis,cis*-HOCOH can decompose into COH and OH, which although highly exothermic (−0.78 eV) is hindered by large activation energy of 1.88 eV.

Another side pathway is hydrogenation of CO to COH. This reaction was shown to be thermodynamically (ΔE = +1.94 eV) and kinetically (E_A = 2.79 eV) impossible. Should COH form *via* decomposition of *cis,cis*-HOCOH, it would be readily hydrogenated into HCOH in a fast exothermic reaction with reaction barrier 0.31 eV and energy of reaction −0.63 eV. Its hydrogenation in CH_2OH has a barrier of 0.63 eV and is only slightly endothermic (+0.21 eV). CH_2OH could only theoretically form from H_2CO, as the reaction barrier equals 1.81 eV. C H_2OH transforms into CH_3OH with reaction barrier 0.71 eV.

3.6.6. Water formation

Water is another product in the hydrogenation of CO_2 into methanol. As discussed above, OH can form in various different elementary reactions. Formation of adsorbed atomic oxygen, however, is not favourable. OH can react with co-adsorbed hydrogen to form water. This reaction is slightly endothermic with energy of reaction +0.36 eV and rather slow with reaction barrier 1.25 eV. Decomposition of OH into O and H is unlikely, as activation energy was calculated to exceed 1.8 eV.

4. Discussion

CCSD(T) results obtained with a sufficiently large basis set are widely used as the benchmark for theoretical calculations of molecular electronic structure and energy. In this manner we calculated the thermodynamic parameters for methanol synthesis and reverse water–gas shift reaction. Experimentally determined enthalpy change for the former reaction is −48.98 kJ/mol and compares favourably with our CCSD(T)/aug-cc-pVQZ value of −51.61 kJ/mol, both at standard ambient conditions. Basis set testing showed that this value is converged with respect to the size of the basis set. The discrepancy is ascribed to the shortcomings of the CCSD(T) method itself – *e.g.* imprecise treatment of triple excitations and neglecting higher excitations, and the accuracy of the experiment. Similar holds true for RWGS with experimental value of +41.16 kJ/mol and theoretical result of +37.71 kJ/mol.

Methanol synthesis is an exothermic reaction with considerable decrease in entropy, as four molecules are ultimately consumed to yield two molecules of products. This competition of enthalpy and entropy favours lower temperatures. Additionally, high pressure pushes the thermodynamic equilibrium towards methanol and water. However, a balance must be struck between the low temperatures desired by thermodynamics of the reaction and higher temperatures needed to reach reasonable reaction rates.

RWGS is of course independent of pressure as the amount of substance does not change in the reaction. There is a net entropy gain in the reaction as products are less symmetric and have more degrees of freedom. For instance, the symmetry number for H_2 and CO_2 is 2 and for CO is 1, while H_2O has C_{2V} symmetry. As there is a competition between the unfavourable enthalpy and favourable entropy change, the reaction gets more favourable with increasing temperature. This is a well-known problem in the methanol synthesis, as higher temperatures, while overall increasing the conversion, guide the reaction towards the production of CO instead of methanol.

There is considerable debate in the literature over the principal route that leads to formation of methanol from carbon dioxide. Most often, the formate route is proposed [3], but several authors argue that other pathways make a significant or even predominant contribution [10]. The situation is further complicated by different theoretical methodologies employed, while experimental techniques have not yet been able to confirm the presence of all intermediates and irrefutably prove or disprove the pathways.

Mostly, formate and RWGS pathways are discussed as the most probable routes for methanol synthesis. There are, however, variations in pathways. Formate pathways may include H_2COOH, which decomposes to CH_2O and OH, or postulate scission of the O–O bond in H_2COO. There is also a possibility for the pathways to cross. For instance HCOO from the formate pathway might be cleaved into HCO (considered a RWGS intermediate) and O.

Our results point towards the conclusion that the formate pathway is prevalent on the $Cu/ZnAl_2O_4$ spinel-type catalyst. Interaction of CO_2 with the surface is weak and non-specific, with the geometry of molecule remaining essentially unperturbed upon approaching the catalyst. We therefore conclude that the reaction most likely proceeds *via* Eley–Rideal mechanism with gaseous CO_2 reacting with adsorbed hydrogen to form HCOO, while *trans*-HOCO cannot form due to large activation barrier. In some studies, HCOO has been considered as a pathway dead end (being strongly bound to the catalyst and having prohibitively large activation energy for further reactions). Our results show, however, that this

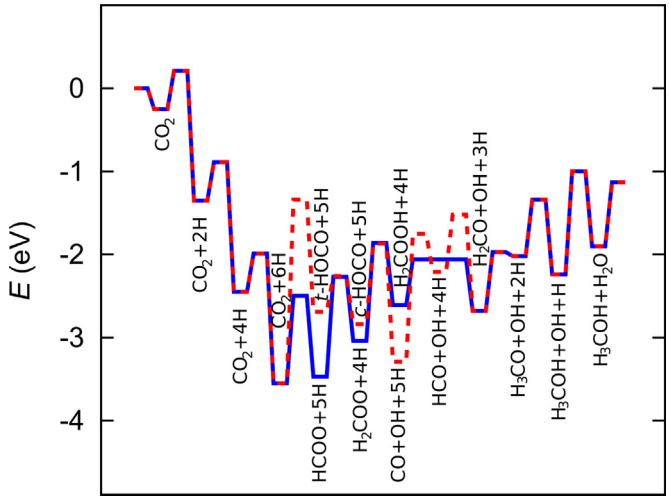

Fig. 8. Calculated potential energy surface for CO_2 hydrogenation to methanol *via* formate (blue solid line) and RWGS (dashed red line) route. (For interpretation of the references to colour in this figure legend, the reader is referred to the web version of this article.)

intermediate is then consecutively hydrogenated into H_2COO and H_2COOH in two slow rate-determining steps with very similar activation energies.

Formation of noticeable quantities of HCOOH can be dismissed on the thermodynamic grounds. Activation energy for its formation from HCOO is smaller than that for the formation of H_2COO, but the reverse reaction is very fast, meaning that HCOOH decomposes before it could react further. Subsequent hydrogenation steps yield CH_2O, H_3CO and ultimately CH_3OH. These steps have lower activation energy than preceding, meaning that they do not determine the reaction rate. Potential energy surface for this pathway is graphically shown in Fig. 8.

The alternative RWGS route is less likely because of the high reaction barrier for the first step, *i.e.* hydrogenation of CO_2 to HOCO. Consequently, CO, HOCOH and COH cannot form. Decomposition of HCOOH to HCO, which could overcome this obstacle, is also kinetically forbidden as HCOOH would with much lower activation barrier rather decompose back into HCOO. Finally, one should take into account the side reactions. CH_2O could theoretically hydrogenate to CH_2OH instead of CH_3O. Activation energy for this alternative step is prohibitively large because CH_3OH is acidic. It is therefore extremely unlikely that it would abstract the aliphatic hydrogen atom first. A similar line of reasoning explains why CH_2O is formed instead of HCOH from HCO, and HCO instead of COH from CO.

These results are comparable to several studies that investigated this reaction on pure Cu and other metallic surfaces, but differ in some subtleties. This is probably due to two main factors. Firstly, effects of Zn and $ZnAl_2O_4$ support are important. This is a well-known fact, evidenced by the design of industrial catalysts as mixtures of Cu, ZnO and alumina. Secondly, by placing active cluster on top of spinel 110 plane, a jagged surface was created, approximating steps and other defects which are known to promote catalytic activity. These effects are neglected when the reaction is studied on simple low Miller index planes on pure metals.

5. Conclusion

CCSD(T) calculations were performed to investigate the thermodynamics and equilibria of CO_2 hydrogenation. Enthalpy, entropy, Gibbs free energy and equilibrium constants of the reaction CO_2 (g) + 3 H_2 (g) → CH_3OH (g) + H_2O (g) and the principal side reaction (reverse water–gas shift reaction) CO_2(g) + H_2 (g) → CO (g) + H_2O (g) were calculated at several temperatures and pressures. CCSD(T) with aug-cc-pVQZ basis set is considered a golden standard in computational chemistry, yielding highly accurate results that are often used as a benchmark.

Furthermore, an exhaustive study of all possible intermediates in the catalysed reaction was carried out. DFT calculations were performed on spinel-type Cu/$ZnAl_2O_4$ catalyst, which is a veracious representation of the industrial catalyst. It was found that the reaction proceeds *via* the formate route. The key intermediates in the reaction are HCOO, H_2COO, H_2COOH, H_2CO and H_3CO. The rate-limiting steps are the formation of H_2COO and H_2COOH. Reverse water–gas shift pathway, proceeding through *t*-HOCO, *c*-HOCO, CO, and HCO is kinetically less likely. Formation of even less stable intermediates (COH, *t,t*-HOCOH, *c,t*-HOCOH, *c,c*-HOCOH, HCHO or CH_2OH) can be dismissed based on our results.

Acknowledgements

Authors gratefully acknowledge financial support by the EU Framework Programme for Research and Innovation Horizon 2020 under Grant agreement no. 637016 (MefCO2) and Slovenian Research Agency (ARRS) through Programme P2-0152. We would like to thank Sir Robert Rep for a wonderful design of the graphical abstract.

Appendix A. Supplementary data

Supplementary data associated with this article can be found, in the online version, at http://dx.doi.org/10.1016/j.apcatb.2017.01.077.

References

[1] C. Song, Global challenges and strategies for control, conversion and utilization of CO_2 for sustainable development involving energy, catalysis, adsorption and chemical processing, Catal. Today 115 (2006) 2–32, http://dx.doi.org/10.1016/j.cattod.2006.02.029.
[2] I. Kasatkin, P. Kurr, B. Kniep, A. Trunschke, R. Schlögl, Role of lattice strain and defects in copper particles on the activity of Cu/ZnO/Al_2O_3 catalysts for methanol synthesis, Angew. Chem. 119 (2007) 7465–7468, http://dx.doi.org/10.1002/ange.200702600.
[3] M. Behrens, F. Studt, I. Kasatkin, S. Kühl, M. Hävecker, F. Abild-Pedersen, S. Zander, F. Girgsdies, P. Kurr, B.-L. Kniep, M. Tovar, R.W. Fischer, J.K. Nørskov, R. Schlögl, M.S. Spencer, I. Kasatkin, P. Kurr, B. Kniep, A. Trunschke, R. Schlögl, M. Behrens, M. Kurtz, H. Wilmer, T. Genger, O. Hinrichsen, M. Muhler, M. Kurtz, J. Yoshihara, C.T. Campbell, P.B. Rasmussen, J. Szanyi, D.W. Goodman, R. Burch, S.E. Golunski, M.S. Spencer, Y. Kanai, T. Watanabe, T. Fujitani, T. Uchijima, J. Nakamura, K. Klier, V. Ponec, W.P.A. Jansen, J.C. Frost, J. Nakamura, Y. Choi, T. Fujitani, K.C. Waugh, P.L. Hansen, M.M. Günter, G.C. Chinchen, P.J. Denny, J.R. Jennings, M.S. Spencer, K.C. Waugh, L.C. Grabow, M. Mavrikakis, Z.-M. Hu, K. Takahashi, H. Nakatsuji, Y. Yang, J. Evans, J.A. Rodriguez, M.G. White, P. Liu, Y. Morikawa, K. Iwata, K. Terakura, N.-Y. Topsøe, H. Topsøe, R.N. d'Alnoncourt, J.D. Grunwaldt, A.M. Molenbroek, N.Y. Topsoe, H. Topsoe, B.S. Clausen, J. Słoczynski, I.A. Fisher, H.C. Woo, A.T. Bell, B.L. Kniep, M. Behrens, M. Behrens, I. Kasatkin, S. Kühl, G. Weinberg, G.C. Chinchen, C.M. Hay, H.D. Vanderwell, K.C. Waugh, O. Hinrichsen, T. Genger, M. Muhler, S.R. Bahn, K.W. Jacobsen, K. Laasonen, A. Pasquarello, R. Car, C. Lee, D. Vanderbilt, M.C. Payne, M.P. Teter, D.C. Allan, T.A. Arias, J.D. Joannopoulos, D. Vanderbilt, B. Hammer, L.B. Hansen, J.K. Nørskov, H.J. Monkhorst, J.D. Pack, G. Kresse, J. Furthmuller, L. Bengtsson, A.A. Peterson, F. Abild-Pedersen, F. Studt, J. Rossmeisl, J.K. Nørskov, The active site of methanol synthesis over Cu/ZnO/Al_2O_3 industrial catalysts, Science 336 (2012) 893–897, http://dx.doi.org/10.1126/science.1219831.
[4] M. Kurtz, N. Bauer, C. Büscher, H. Wilmer, O. Hinrichsen, R. Becker, S. Rabe, K. Merz, M. Driess, R.A. Fischer, M. Muhler, New synthetic routes to more active Cu/ZnO catalysts used for methanol synthesis, Catal. Lett. 92 (2004) 49–52, http://dx.doi.org/10.1023/B:CATL.0000011085.88267.a6.
[5] G.C. Chinchen, K.C. Waugh, D.A. Whan, The activity and state of the copper surface in methanol synthesis catalysts, Appl. Catal. 25 (1986) 101–107, http://dx.doi.org/10.1016/S0166-9834(00)81226-9.
[6] R. Burch, S.E. Golunski, M.S. Spencer, J.C.J. Bart, R.P.A. Sneeden, G.C. Chinchen, P.J. Denny, J.R. Jennings, M.S. Spencer, K.C. Waugh, G. Ghiotti, F. Boccuzzi, K. Klier, A. Amara, M. Bettahar, D. Olivier, G.C. Chinchen, K.C. Waugh, D.A. Whan, G.C. Chinchen, P.J. Denny, D.G. Parker, M.S. Spencer, D.A. Whan, G.C. Chinchen,

P.J. Denny, D.G. Parker, G.D. Short, M.S. Spencer, K.C. Waugh, D.A. Whan, D.H.S. Ying, R.J. Madix, T. Tagawa, G. Pleizer, Y. Amenomiya, S. Kinnaird, G. Webb, G.C. Chinchen, M. Bowker, R.A. Hadden, H. Houghton, J.N.K. Hyland, K.C. Waugh, J.C. Frost, B. Denise, R.P.A. Sneeden, B. Beguin, O. Cherifi, P.B. Wells, W.R.A.M. Robinson, J.C. Mol, R. Burch, R.J. Chappell, R. Burch, R.J. Chappell, S.E. Golunski, M.E. Fakley, J.R. Jennings, M.S. Spencer, J. Saussey, J.C. Lavalley, R. Burch, R.J. Chappell, S.E. Golunski, E. Baumgarten, C. Lentes-Wagner, R.W.C.C. Wagner Jr., G.M. Pajonk, S.J. Teichner, P.R. Dennison, K.J. Packer, M.S. Spencer, K.C. Waugh, R.A. Hadden, H.D. Vandervell, K.C. Waugh, G. Webb, S. Kinnaird, G. Webb, G.C. Chinchen, M. Bowker, H. Houghton, K.C. Waugh, J.B. Bulko, R.G. Herman, K. Klier, G.W. Simmons, G.J.J. Bartley, R. Burch, D.L. Roberts, G.L. Griffin, D. Duprez, J. Barbier, J.F. Hamida, M. Bettahar, D.J.C. Yates, The role of copper and zinc oxide in methanol synthesis catalysts, J. Chem. Soc. Faraday Trans. 86 (1990) 2683, http://dx.doi.org/10.1039/ft9908602683.

[7] J. Nakamura, T. Uchijima, Y. Kanai, T. Fujitani, The role of ZnO in Cu/ZnO methanol synthesis catalysts, Catal. Today 28 (1996) 223–230, http://dx.doi.org/10.1016/0920-5861(95)00240-5.

[8] M. Behrens, S. Zander, P. Kurr, N. Jacobsen, J. Senker, G. Koch, T. Ressler, R.W. Fischer, R. Schlögl, Performance improvement of nanocatalysts by promoter-induced defects in the support material: methanol synthesis over Cu/ZnO:Al, J. Am. Chem. Soc. 135 (2013) 6061–6068.

[9] M.M. Günter, T. Ressler, B. Bems, C. Büscher, T. Genger, O. Hinrichsen, M. Muhler, R. Schlögl, Implication of the microstructure of binary Cu/ZnO catalysts for their catalytic activity in methanol synthesis, Catal. Lett. 71 (2001) 37–44, http://dx.doi.org/10.1023/A:1016696022840.

[10] Y.-F. Zhao, Y. Yang, C. Mims, C.H.F. Peden, J. Li, D. Mei, Insight into methanol synthesis from CO_2 hydrogenation on Cu(111): complex reaction network and the effects of H_2O, J. Catal. 281 (2011) 199–211, http://dx.doi.org/10.1016/j.jcat.2011.04.012.

[11] L.C. Grabow, M. Mavrikakis, Mechanism of methanol synthesis on Cu through CO_2 and CO hydrogenation, ACS Catal. 1 (2011) 365–384.

[12] F. Studt, F. Abild-Pedersen, J.B. Varley, J.K. Nørskov, CO and CO_2 hydrogenation to methanol calculated using the BEEF-vdW functional, Catal. Lett. 143 (2013) 71–73, http://dx.doi.org/10.1007/s10562-012-0947-5.

[13] Y. Yang, J. Evans, J.A. Rodriguez, M.G. White, P. Liu, Fundamental studies of methanol synthesis from CO_2 hydrogenation on Cu(111), Cu clusters, and Cu/ZnO(0001−), Phys. Chem. Chem. Phys. 12 (2010) 9909, http://dx.doi.org/10.1039/c001484b.

[14] Y. Yang, M.G. White, P. Liu, Theoretical study of methanol synthesis from CO_2 hydrogenation on metal-doped Cu(111) surfaces, J. Phys. Chem. C 116 (2011) 248–256.

[15] H. Nakatsuji, Z.-M. Hu, Mechanism of methanol synthesis on Cu(100) and Zn/Cu(100) surfaces: comparative dipped adcluster model study, Int. J. Quantum Chem. 77 (2000) 341–349, doi:10.1002/(SICI)1097-461X(2000)77:1<341::AID-QUA33>3.0.CO;2-T.

[16] R.J. Bartlett, G.D. Purvis, Many-body perturbation theory, coupled-pair many-electron theory, and the importance of quadruple excitations for the correlation problem, Int. J. Quantum Chem. 14 (1978) 561–581, http://dx.doi.org/10.1002/qua.560140504.

[17] J.A. Pople, R. Krishnan, H.B. Schlegel, J.S. Binkley, Electron correlation theories and their application to the study of simple reaction potential surfaces, Int. J. Quantum Chem. 14 (1978) 545–560, http://dx.doi.org/10.1002/qua.560140503.

[18] J.A. Pople, M. Head-Gordon, K. Raghavachari, Quadratic configuration interaction. A general technique for determining electron correlation energies, J. Chem. Phys. 87 (1987) 5968, http://dx.doi.org/10.1063/1.453520.

[19] G.D. Purvis, R.J. Bartlett, A full coupled-cluster singles and doubles model: the inclusion of disconnected triples, J. Chem. Phys. 76 (1982) 1910–1918, http://dx.doi.org/10.1063/1.443164.

[20] G.E. Scuseria, C.L. Janssen, H.F. Schaefer, An efficient reformulation of the closed-shell coupled cluster single and double excitation (CCSD) equations, J. Chem. Phys. 89 (1988) 7382, http://dx.doi.org/10.1063/1.455269.

[21] G.E. Scuseria, H.F. Schaefer, Is coupled cluster singles and doubles (CCSD) more computationally intensive than quadratic configuration interaction (QCISD)? J. Chem. Phys. 90 (1989) 3700, http://dx.doi.org/10.1063/1.455827.

[22] R.A. Kendall, T.H. Dunning, R.J. Harrison, Electron affinities of the first-row atoms revisited. Systematic basis sets and wave functions, J. Chem. Phys. 96 (1992) 6796, http://dx.doi.org/10.1063/1.462569.

[23] J.T.H. Dunning, K.A. Peterson, A.K. Wilson, Gaussian basis sets for use in correlated molecular calculations. X. The atoms aluminum through argon revisited, J. Chem. Phys. 114 (2001) 9244–9253, http://dx.doi.org/10.1063/1.1367373.

[24] M.J. Frisch, G.W. Trucks, H.B. Schlegel, G.E. Scuseria, M.A. Robb, J.R. Cheeseman, G. Scalmani, V. Barone, B. Mennucci, G.A. Petersson, H. Nakatsuji, M. Caricato, X. Li, H.P. Hratchian, A.F. Izmaylov, J. Bloino, G. Zheng, J.L. Sonnenberg, M. Hada, M. Ehara, K. Toyota, R. Fukuda, J. Hasegawa, M. Ishida, T. Nakajima, Y. Honda, O. Kitao, H. Nakai, T. Vreven, J.A. Montgomery Jr., J.E. Peralta, F. Ogliaro, M. Bearpark, J.J. Heyd, E. Brothers, K.N. Kudin, V.N. Staroverov, R. Kobayashi, J. Normand, K. Raghavachari, A. Rendell, J.C. Burant, S.S. Iyengar, J. Tomasi, M. Cossi, N. Rega, J.M. Millam, M. Klene, J.E. Knox, J.B. Cross, V. Bakken, C. Adamo, J. Jaramillo, R. Gomperts, R.E. Stratmann, O. Yazyev, A.J. Austin, R. Cammi, C. Pomelli, J.W. Ochterski, R.L. Martin, K. Morokuma, V.G. Zakrzewski, G.A. Voth, P. Salvador, J.J. Dannenberg, S. Dapprich, A.D. Daniels, Ö. Farkas, J.B. Foresman, J. V Ortiz, J. Cioslowski, D.J. Fox, Gaussian 09 Revision E.01, (n.d.) http://gaussian.com/g09citation/.

[25] D.A. McQuarrie, Statistical Mechanics, 6th ed., University Science Books, Sausalito, CA, 2000.

[26] A. Kokalj, Computer Graphics and Graphical User Interfaces as Tools in Simulations of Matter at the Atomic Scale, Comput. Mat. Sci. 28 (2003) 155–168, http://dx.doi.org/10.1016/S0927-0256(03)00104-6.

[27] A. Kokalj, XCrySDen – a new program for displaying crystalline structures and electron densities, J. Mol. Graph. Model. 17 (1998), 176–179, 215–216 (accessed 26.07.16).

[28] J.P. Perdew, K. Burke, M. Ernzerhof, Generalized gradient approximation made simple, Phys. Rev. Lett. 77 (1996) 3865–3868, http://dx.doi.org/10.1103/PhysRevLett.77.3865.

[29] J.P. Perdew, K. Burke, M. Ernzerhof, Generalized Gradient approximation made simple [Phys. Rev. Lett. 77 3865 (1996)], Phys. Rev. Lett. 78 (1997), http://dx.doi.org/10.1103/PhysRevLett.78.1396, 1396-1396.

[30] S. Grimme, Semiempirical GGA-type density functional constructed with a long-range dispersion correction, J. Comput. Chem. 27 (2006) 1787–1799, http://dx.doi.org/10.1002/jcc.20495.

[31] V. Barone, M. Casarin, D. Forrer, M. Pavone, M. Sambi, A. Vittadini, Role and effective treatment of dispersive forces in materials: polyethylene and graphite crystals as test cases, J. Comput. Chem. 30 (2009) 934–939, http://dx.doi.org/10.1002/jcc.21112.

[32] H.J. Monkhorst, J.D. Pack, Special points for Brillouin-zone integrations, Phys. Rev. B 13 (1976) 5188–5192, http://dx.doi.org/10.1103/PhysRevB.13.5188.

[33] L. Bengtsson, Dipole correction for surface supercell calculations, Phys. Rev. B 59 (1999) 12301–12304, http://dx.doi.org/10.1103/PhysRevB.59.12301.

[34] G. Mills, H. Jónsson, G.K. Schenter, Reversible work transition state theory: application to dissociative adsorption of hydrogen, Surf. Sci. 324 (1995) 305–337, http://dx.doi.org/10.1016/0039-6028(94)00731-4.

[35] G. Henkelman, B.P. Uberuaga, H. Joínsson, A climbing image nudged elastic band method for finding saddle points and minimum energy paths, J. Chem. Phys. 113 (2000) 9901, http://dx.doi.org/10.1063/1.1329672.

[36] N. Ahmed, Y. Shibata, T. Taniguchi, Y. Izumi, Photocatalytic conversion of carbon dioxide into methanol using zinc–copper–M(III) (M=aluminum, gallium) layered double hydroxides, J. Catal. 279 (2011) 123–135, http://dx.doi.org/10.1016/j.jcat.2011.01.004.

[37] D.R. Burgess, Thermochemical Data, in: P.J. Linstrom, W.G. Mallard (Eds.), NIST Chem. WebBook, NIST Stand. Ref. Database Number 69, National Institute of Standards and Technology, Gaithersburg, MD, 2016.

[38] J. Papavasiliou, G. Avgouropoulos, T. Ioannides, Combined steam reforming of methanol over Cu–Mn spinel oxide catalysts, J. Catal. 251 (2007) 7–20, http://dx.doi.org/10.1016/j.jcat.2007.07.025.

[39] J. Schumann, A. Tarasov, N. Thomas, R. Schlögl, M. Behrens, Cu,Zn-based catalysts for methanol synthesis: on the effect of calcination conditions and the part of residual carbonates, Appl. Catal. A: Gen. 516 (2016) 117–126, http://dx.doi.org/10.1016/j.apcata.2016.01.037.

[40] S.D. Jones, L.M. Neal, H.E. Hagelin-Weaver, Steam reforming of methanol using Cu–ZnO catalysts supported on nanoparticle alumina, Appl. Catal. B: Environ. 84 (2008) 631–642, http://dx.doi.org/10.1016/j.apcatb.2008.05.023.

[41] Y. Wang, M. Zhou, T. Wang, G. Xiao, Conversion of furfural to cyclopentanol on Cu/Zn/Al catalysts derived from hydrotalcite-like materials, Catal. Lett. 145 (2015) 1557–1565, http://dx.doi.org/10.1007/s10562-015-1539-y.

[42] M. Behrens, I. Kasatkin, S. Kühl, G. Weinberg, Phase-pure Cu,Zn,Al hydrotalcite-like materials as precursors for copper rich $Cu/ZnO/Al_2O_3$ catalysts, Chem. Mater. 22 (2010) 386–397, http://dx.doi.org/10.1021/cm9029165.

[43] K.E. Sickafus, J.M. Wills, N.W. Grimes, Structure of Spinel, J. Am. Chem. Soc. 82 (2004) 3279–3292, http://dx.doi.org/10.1111/j.1151-2916.1999.tb02241.x.

[44] P.B. Rasmussen, M. Kazuta, I. Chorkendorff, Synthesis of methanol from a mixture of H_2 and CO_2 on Cu(100), Surf. Sci. 318 (1994) 267–280, http://dx.doi.org/10.1016/0039-6028(94)90101-5.

[45] X.-K. Gu, W.-X. Li, First-principles study on the origin of the different selectivities for methanol steam reforming on Cu(111) and Pd(111), J. Phys. Chem. C 114 (2010) 21539–21547.

[46] P.R. Schreiner, H.P. Reisenauer, Spectroscopic identification of dihydroxycarbene, Angew. Chem. Int. Ed. 47 (2008) 7071–7074, http://dx.doi.org/10.1002/anie.200802105.

[47] Z.-J. Zuo, L. Wang, L.-M. Yu, P.-D. Han, W. Huang, Experimental and theoretical studies of ethanol synthesis from syngas over CuZnAl catalysts without other promoters, J. Phys. Chem. C 118 (2014) 12890–12898.

[48] L.I. Bendavid, E.A. Carter, CO_2 adsorption on $Cu_2O(111)$: a DFT+U and DFT-D study, J. Phys. Chem. C 117 (2013) 26048–26059.